Title
Wafer-Scale CMP Modeling of With-in Wafer Non-Uniformity

Authors
Luo, Jianfeng
Dornfeld, David A

Publication Date
2003-06-01

Wafer-Scale CMP Modeling of With-in Wafer Non-Uniformity

Jianfeng Luo
Sponsored by NSF and UC SMART

Abstract— In this report, the with-in wafer non-uniformity (WIWNU) of material removal rate and its optimization are discussed from both the machine side and consumable side. At the machine side, the pressure and velocity distribution are the major reasons for the non-uniform material removal rate across the wafer. The velocity distributions for the rotational type and linear type of machines are analyzed systematically. The rotational part of the velocity is the contributor of the velocity non-uniformity. The pressure non-uniformity in both cases of the solid-solid contact and the solid-fluid-solid contact are discussed. Adding the retaining ring is an effective way to reduce the pressure non-uniformity at the edge of the wafer in the solid-solid contact mode. In the solid-fluid-solid contact mode, the friction coefficient is identified as the major contributor to the non-uniformity. A process window of pressure and velocity in terms of small non-uniformity can be obtained by combining the model proposed in this report and the Stribeck curve of the friction coefficients. At the consumable side, a systematic method is proposed to optimize the WIWNU in solid-solid contact mode, based on the material removal model developed in previous works [5, 6, 7]. The basic idea is to reduce the sensitivity of the material removal on pressure and velocity distribution.

Keywords: WIWNU, Velocity Distribution, Pressure Distribution, Solid-Solid Contact, Solid-Fluid-Solid Contact, Friction Coefficients, Consumable Effects, Modeling, Optimization.

1. Introduction

The with-in wafer non-uniformity (WIWNU) of the material removal rate across the wafer has long been a concern in chemical mechanical planarization (CMP). For instance, the edge effects, namely, the rapid variation of the material removal rate at the edge, require an exclusion of the wafer edge after CMP. This reduces the yields of the process. The uneven material removal rates across the wafer will bring the over-polishing in the faster removal regions in the shallow trench isolation (STI) and copper damascene processes. This causes a degeneration of the circuit performance in that area. In addition, WIWNU will bring a systematic variation of the circuit performance across the wafer. A better understanding of the formation mechanism of the WIWNU will be able to increase the yields and help to optimize the circuit performances.

While the maximum, minimum, and average material removal rate MRR_{max}, MRR_{min} and MRR_{avg} over the wafer surface are known, the WIWNU can be expressed as follows:

$$\text{WIWNU} = \frac{MRR_{max} - MRR_{min}}{MRR_{avg}} \times 100\%. \tag{1}$$

The non-uniform removal rate across the wafer in CMP can be attributed to the uneven distribution of a number of parameters such as the temperature and slurry distributions. However, it is believed that the distributions of the pressure P and velocity V are the two major contributors. Substitution of the revised Preston's Equation of material removal rate $MRR = K_e PV + MRR_0$ where K_e and MRR_0 are two experimental fitting parameters, into Equation 1 yields

$$\text{WIWNU}= \frac{K_e(PV)_{\max} + MRR_0 - K_e(PV)_{\min} - MRR_0}{K_e(PV)_{avg} + MRR_0} = \frac{K_e\left[(PV)_{\max} - (PV)_{\min}\right]}{MRR_{avg}} \tag{2}$$

From Equation 2 there are basically two methods to optimize WIWNU. One is to reduce the non-uniformity of the pressure and velocity distribution, or reduce the value of $PV_{\max}$-$PV_{\min}$ in Equation 2. This may be realized through the optimization of machine design, especially, the polishing head and platen design. Another method is to reduce the sensitivity of MRR to the pressure and velocity distribution. This sensitivity can be adjusted through the fitting parameters K_e and MRR_0 in Equation 2, which are determined by the consumable parameters. In this report, models are developed from both sides. First, analytical and numerical models are proposed for the prediction of velocity distributions, for both rotational type and linear type of CMP machine, and pressure distributions, in both solid-solid contact and solid-fluid-solid contact modes. These models can help to optimize the WIWNU from the viewpoint of the machine configuration. Then, a systematic method using the particle scale MRR models developed in previous work [5, 6, 7] is proposed to optimize the non-uniformity from the viewpoint of consumable effects.

2. CMP configurations and velocity distribution

The velocity distribution is a function of the configurations of the CMP machine. There are typically two different CMP configurations, one, rotational type and the other, linear type. In the rotational type of machines, the wafer is affixed to a wafer carrier (via back-pressure), and pressed faced-down on a rotating platen holding a polymeric polishing pad, as illustrated in Figure 1. The CMP equipments by Applied Materials Inc., Ebarra Tech. and Novellus Inc. fall into this category. In the linear type, a polishing head is rotated above a belt made of polymer materials, which is driven by motors to move linearly in one direction. The configuration of linear type of CMP machine is schematically shown in Figure 2. The movement of the wafer relative to the pad/belt can

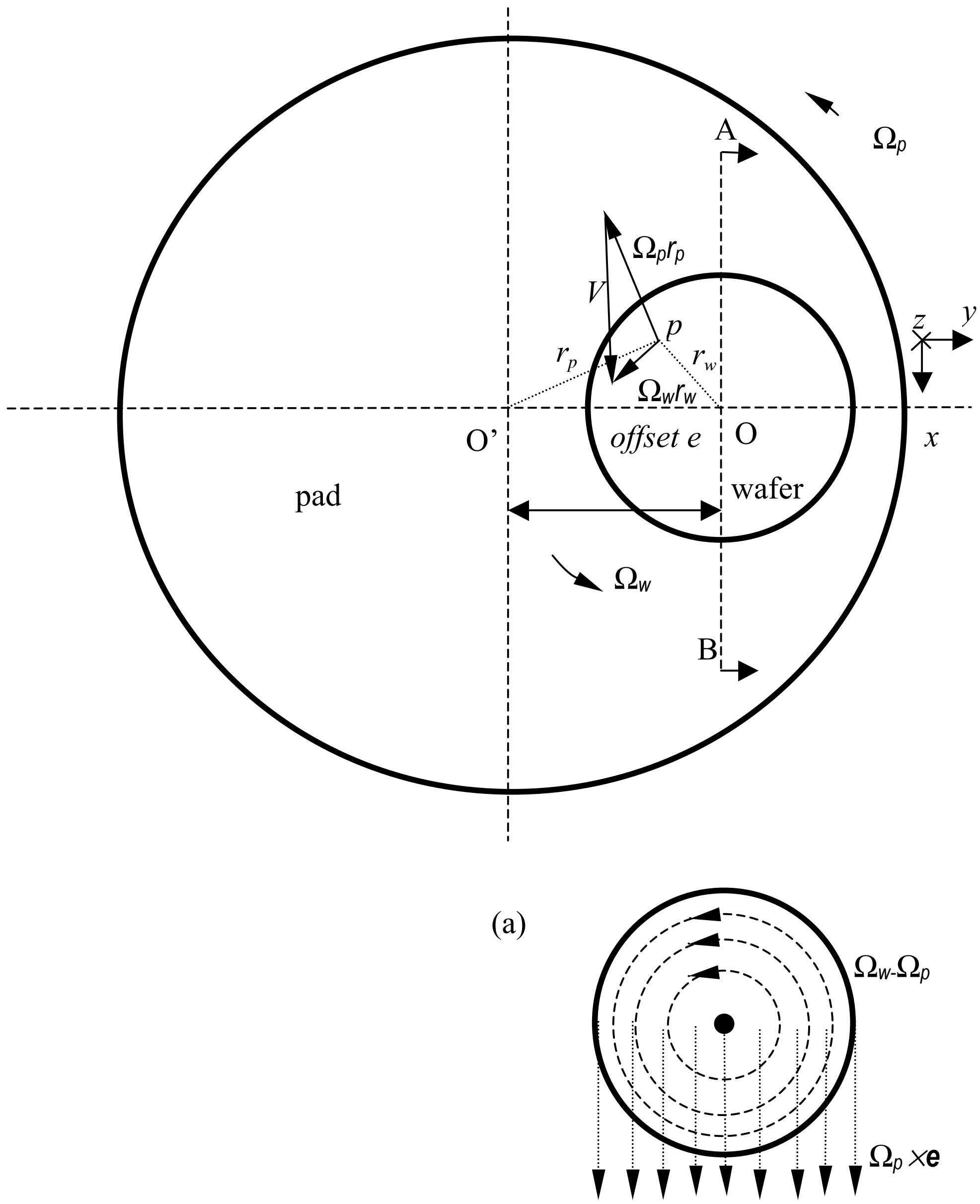

(b)

Figure 1. Top view of a rotational type of CMP machine and velocity distribution over the wafer surface.

be separated into two components: one, a rotation of the wafer around its center and, the other, a linear translation of the wafer. This is apparent for the linear type of configuration, where the speed of the rotation is equal to the polishing head rotation speed and the speed of the translation is equal to the linear velocity of the belt, Figure 2. It is not so apparent for the rotational type of machine. The following analysis shows how

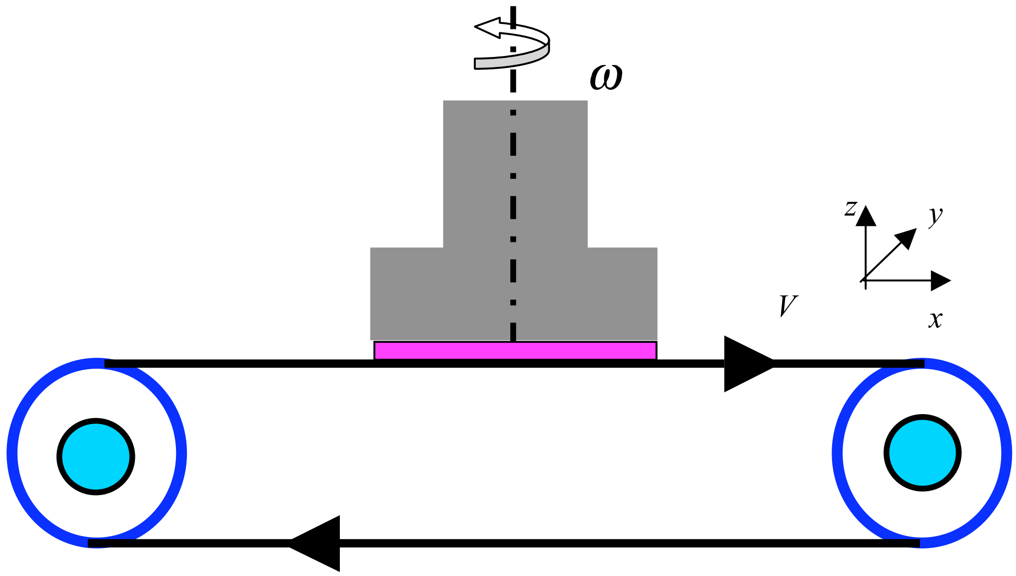

Figure 2. Side view of linear type CMP Machine.

the relative velocity over wafer surface can be decomposed into these two parts for a rotational type of machine.

Let us consider a point p on the wafer surface in a rotational type of machine; see Figure 1. The relative velocity of the wafer to the platen over there can be expressed in vector form as

$$
\begin{aligned}
\vec{V}(p) &= \vec{\Omega}_w \times \vec{r}_w - \vec{\Omega}_p \times \vec{r}_p = \Omega_w(\vec{k} \times \vec{r}_w) - \Omega_p(\vec{k} \times \vec{r}_p) \\
&= -\Omega_p(\vec{k} \times \vec{r}_p) + \Omega_p(\vec{k} \times \vec{r}_w) + (\Omega_w - \Omega_p)(\vec{k} \times \vec{r}_w) \\
&= \Omega_p[\vec{k} \times (\vec{r}_w - \vec{r}_p)] + (\Omega_w - \Omega_p)(\vec{k} \times \vec{r}_w) = -\Omega_p(\vec{k} \times \vec{e}) + (\Omega_w - \Omega_p)(\vec{k} \times \vec{r}_w)
\end{aligned}
$$

where Ω_p, Ω_w are the rotation speeds of the platen/pad and wafer, respectively, r_p , r_w are the distances between the point p and the pad center O' and the wafer center O, respectively and e the offset distance between the pad and wafer centers. All symbols with an arrow denote their vector forms. The $\vec{k}$ represents a unit vector in the z direction perpendicular to the rotation plane.

The above equation shows apparently that the relative movement of wafer over pad is composed of two parts: (1) a *translation* with constant velocity $\Omega_p \times \boldsymbol{e}$ independent of the location of p, where Ω_p is the rotation speed of pad/platen and e the offset between the centers of the platen and wafer; and (2) a *rotation* with constant rotation speed Ω_w-Ω_p, where Ω_w is the rotation speed of wafer/polishing head. Therefore, in terms of velocity distribution, the rotational type of machine with a wafer rotation speed Ω_w and a platen rotation speed Ω_p can be resembled by a linear type of machine with an *effective* wafer rotation speed $\omega = \Omega_w - \Omega_p$ and an *effective* belt speed $V = \Omega_p \times \boldsymbol{e}$, Figure 1 (b) & Figure 2.

The rotation component of the relative velocity is the contributor of the velocity non-uniformity for both rotational and linear type of machines. A smaller rotation speed and a larger translation speed are preferred in terms of smaller velocity non-uniformity. For a rotational type of CMP configurations, this indicates a larger platen velocity Ω_p, a larger wafer-platen center offset e and closer platen and head rotation speeds. When the rotational speed is zero, (In the case of the rotational type of machine, this implies that the rotation speed of the head is equal to the rotation speed of the platen.) the relative movement is a pure translation and therefore there is no velocity non-uniformity. However, there is a tradeoff. While a smaller rotational speed benefits the non-uniformity, with no wafer rotations, the material removal at each single point p cannot be averaged out. Therefore, a sufficiently large rotation speed (for rotational type of machine, a sufficiently large difference between the rotation speeds of the wafer and platen) will be needed. In consideration of this tradeoff, the conditions that an optimal velocity combination should satisfy can be obtained following the following procedures:

1. For a linear type of machine: Let the linear velocity as large as possible and the rotational speed of the head is as small as possible. However, don't let the rotational speed be zero to ensure the material removal is averaged out for each point.
2. For a rotational type of machine: Let the platen rotation speed as large as possible and the difference between the rotation speeds of the platen and head as small as possible. However, don't let the rotational speed of the platen equal to the rotational speed of to ensure the material is averaged out for each point.

The friction force due to the relative movement of the wafer can correspondingly be decomposed into two parts; one, the shear force f_1 along the direction of the translation and the other, the shear force f_2 along the direction of the rotation. The shear force f_1 leads to a gimbals moment of the wafer in the x-z plane as shown in Figures 1 & 2, and the shear force f_2 leads to a rotation moment. The rotation moment will be balanced by the motor driving the polishing head. The gimbals moment, however, needs to be balanced by an asymmetric distribution of the normal pressure. The magnitude of the moment, or the shear force, will have an influence on the normal average pressure distribution, specially, in the case of solid-fluid-solid contact. This will be addressed in later sections.

In terms of the space occupied, it is seen that the linear type of machine is advantageous over the rotational type of machine. The width of the machine in the y direction shown in Figure 2 is in the range of the wafer size. For a rotational type of machine, however, this width, Figure 1, should be at least equal to the wafer radius plus the offset distance e and the platen radius, which is much larger than that in the linear type of machines. The current trend in semiconductor manufacturing is to increase the wafer diameter from 200mm (8inch) to 300mm (12inch) to save the manufacturing costs. In the 300mm era, the rotational type of configuration may not be desired considering the large space occupied by the machine.

It is noted that recently some novel configurations of CMP machines, such as a reverse linear type of machine, where the belt moves in both directions, and a web type of CMP machine, where the head rotates not only around its own center, but the platen center has been announced by suppliers such as NuTool and Applied Materials. The velocity distribution in them is more complicated than that in the above conventional configurations. A similar dynamics analysis as in this section, however, can be done for them and it is ignored here.

3. Pressure distribution

In the following sections, the pressure distribution over the wafer-pad/belt interface is modeled. Two process conditions may exit. One is solid-solid contact, when the down pressure is large and the relative velocity is small. The other is solid-fluid-solid contact, when the down pressure is small and the relative velocity is large. We first consider the case of the solid-solid contact. It is the favorite condition, due to its better planarization ability. Then the solid-fluid-solid contact case is considered. This contact mode may be preferred in low-k CMP. In CMP of low-k dielectrics, usually soft polymer materials, an aggressive contact between low-k layer and pad/belt will cause delamination of the metals and dielectrics. The existence of a thin fluid film over wafer-pad interface may reduce the delamination due to a less aggressive contact between the pad, abrasives and the wafer.

3.1. Solid-solid contact

In the solid-solid contact mode, the governing equation of the wafer and pad deformation is

$$\sigma_{ij} = \frac{2G\nu}{1-2\nu}\delta_{ij}\varepsilon_{kk} + 2G\varepsilon_{ij} \tag{3}$$

where σ_{ij}, ε_{ij}, G and υ are the stress tensor, strain tensor, shear modulus and Poisson's ratio, and δ_{ij} is the Kronecher delta symbol. The wafer and pad are assumed to be homogeneous isotropic materials. The normal pressure/stress distribution $P(x)$ on the wafer surface arises mainly from two sources: (1) down pressure exerted on the wafer top surface, and (2) friction force due to the relative motion of wafer and pad. As mentioned in the last section, for both linear and rotational type machines, the friction force can be separated into two parts, one, a force in the direction of the translation, and the other, a force in the direction of the rotation. The effect of the friction force due to the relative rotation is equal to a pure shear moment, which is balanced by the motor driving the polishing head. It does not have influence on the normal pressure. The friction force in the translation direction has an influence on the pressure distribution. It will be shown by analytical analysis that its effects on the normal pressure distribution can be neglected for the solid-solid contact mode.

3.1.1. Rigid flat punch indentation model

First, a rigid flat punch indentation model by Johnson [1] can be used to model the normal pressure distribution over the wafer-pad interface. This model is a two-dimensional plain strain model with the assumption that the punch does not tilt and therefore the interface remains parallel to the undeformed surface of the solid. The wafer can be modeled as the rigid flat punch and the pad can be modeled as the elastic half-space, as shown in Figure 3. The pressure distribution functions for frictionless punch and sliding punch are proposed as:

$$P(x)=\frac{P_{app}}{\pi(R^2-x^2)^{1/2}}, \tag{4}$$

and

$$P(x)=\frac{P_{app}\cos(\pi\gamma)}{\pi(R^2-x^2)^{1/2}}\left(\frac{R+x}{R-x}\right)^{\gamma}, \tag{5}$$

respectively, where P_{app} is the force applied on the wafer top surface, R the radius of the wafer, $\cot\pi\gamma=-\frac{2(1-\upsilon)}{f(1-2\upsilon)}$, f the friction coefficient of the wafer-pad interface and υ the Poisson's ratio of the pad material. Figure 4(a) shows the simulation results of the

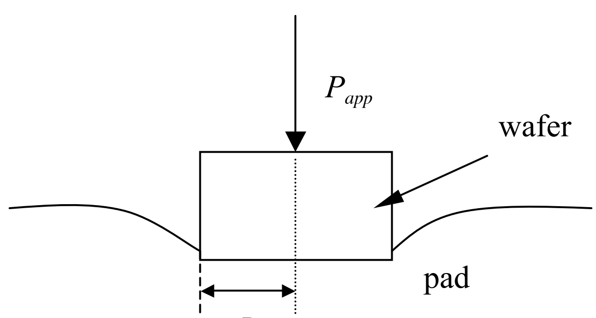

Figure 3. Rigid flat punch model of wafer-pad contact.

pressure distribution across a 300 mm wafer under different friction coefficients. P in the figure is the average pressure across the wafer. This pressure distribution is asymmetric when the friction coefficient is larger than zero. It is also observed that the pressure is increased rapidly at the edge of the wafer. This is due to the fact that the edge is a singular point in Equations (4) and (5). The material removal is usually increased sharply at the wafer edge. This may be attributed to the pressure singularity. Considering the average effects of the rotation component of the velocity distribution, the average pressure distribution should be given by the following equation:

$$Avg(P(x)) = (P(x) + P(-x)) \; / 2 \qquad (6)$$

The simulation results of the average pressure distribution is shown schematically in Figure 4(b). There is not apparent change when the friction coefficient is changed from 0

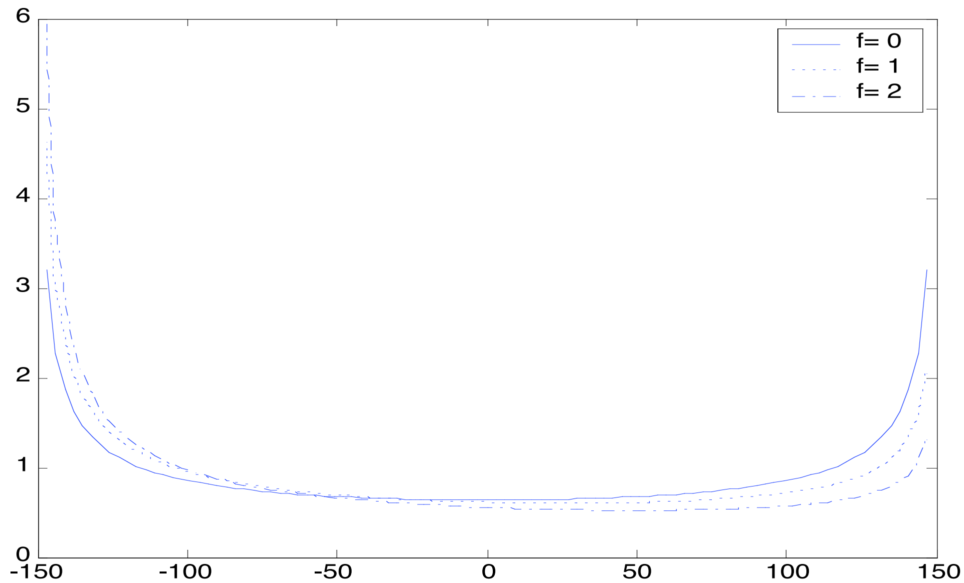

Figure 4(a) Pressure across the wafer under different friction coefficients f based on rigid flat punch model.

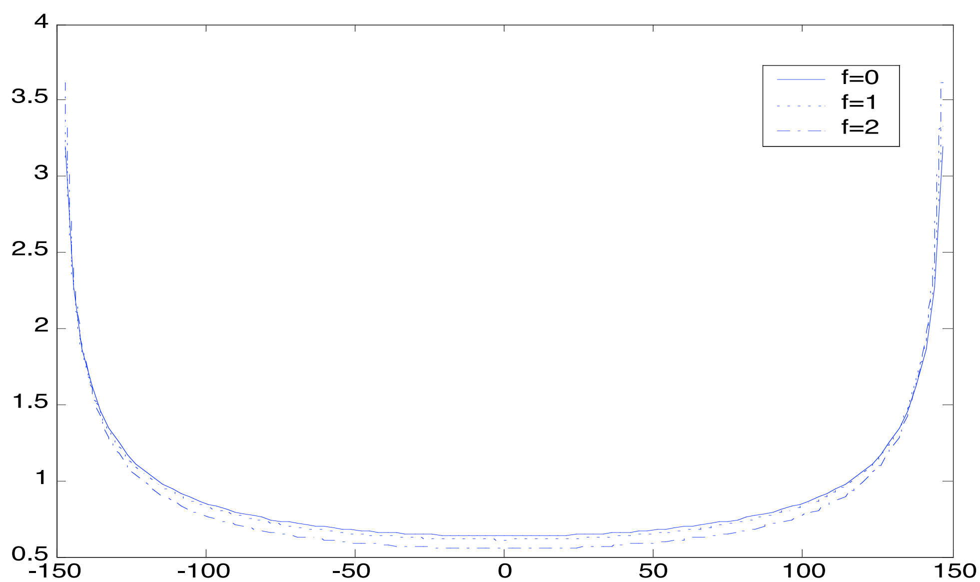

Figure 4(b). Average pressure across the wafer under different friction coefficients f based on rigid flat punch model.

to 1. When the friction coefficient is changed from 1 to 2, the average pressure change is more apparent but is still as small as $0.1P$. Based on the experimental data of Moon [2], the friction coefficients in CMP are usually in the range of 0~ 1. This indicates that the effects of the shear stress may be ignored in the normal pressure prediction.

3.1.2. Boundary Element Model

The above flat rigid punch model does not consider the elastic deformation of the wafer. The geometry parameters such as the wafer thickness and pad thickness are not included. Therefore, it cannot capture some of the critical features of the interface pressure profile, say, the complicated variance of the pressure distribution at the wafer edge. Moreover, this model cannot provide flexibility on polishing head design. A numerical model is therefore preferred. Instead of the conventional finite element model, a two dimensional boundary element model is chosen in this work for its lower requirements on computer memory and faster computation speed in thin structure analysis [3]. Another advantage of boundary element model is its minimum remeshing requirement for geometry optimization met in our simulations.

The boundary element model is shown schematically in Figure 5. It is the cross section along A-B, as shown in Figure 2. The wafer is pressed over the pad by a pressure P distributed uniformly over the wafer top surface. The wafer diameter is 300 mm. The size of the platen/pad is set as 900 mm. This parameter is selected for the rotation type of machine. For a linear type of machine, this parameter may be smaller. Realizing from the punch model that the pressure increases sharply at the wafer edge, a retaining ring can be put around the wafer to adjust the pressure distribution. The ring size is fixed at 10 mm. A gap exists between the wafer and the retaining ring. In our simulation, it ranges from 0 to 2 mm. The pressure over the retaining ring is adjusted from 0 to $4P$. The ring is assumed to be rigid in the current model. Therefore, the pressure over the ring can be applied directly over the pad surface. The wafer and pad Young's modulus are set at 100 GPa and 10 MPa, respectively, which are closed to those met practically.

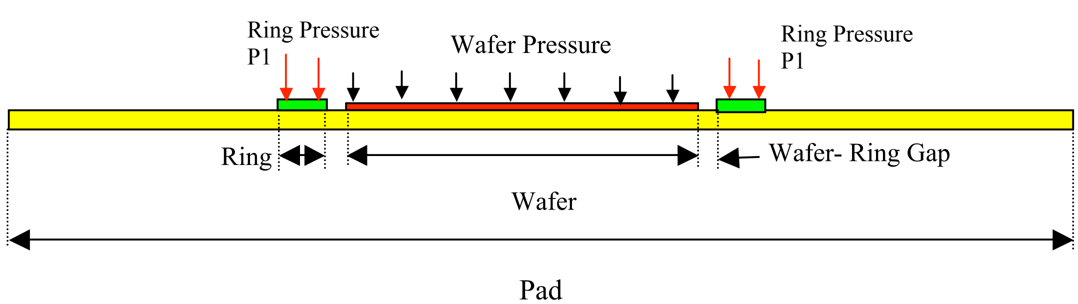

Figure 5. Boundary element model for pressure distribution analysis.

The friction force over the wafer-pad interface is assumed to be zero. This zero friction assumption is based on two considerations. First, from the rigid flat punch model, the friction coefficient does not have apparent influence on the average normal pressure distribution. Therefore, a zero friction assumption should not cause much changes of the results. Second, the contact model with non-zero friction coefficient is very complicated and cannot be implemented by the current boundary element code yet.

Figure 6 shows the simulation results of pressure distribution at the edge of the wafer

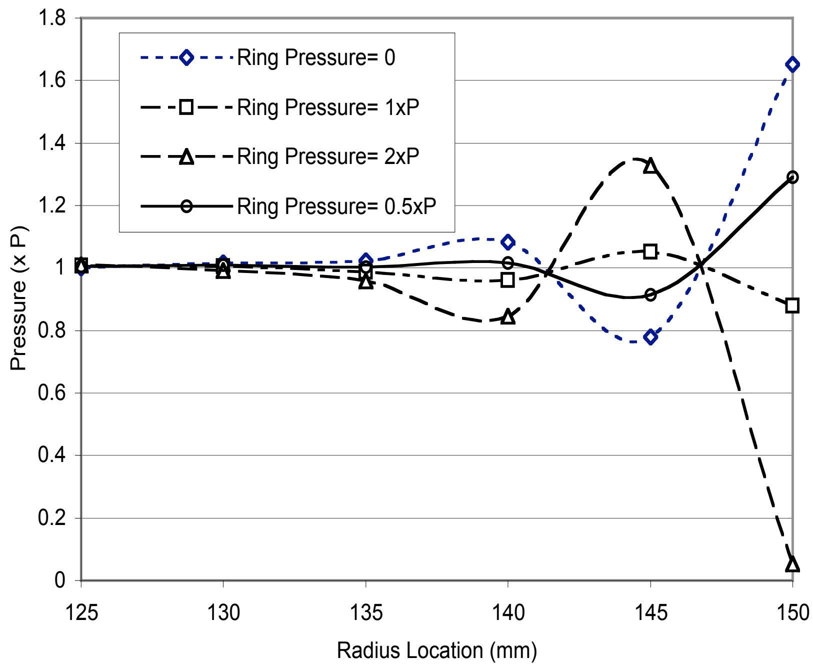

Figure 6. Pressure distribution with different ring pressure when the gap is zero.

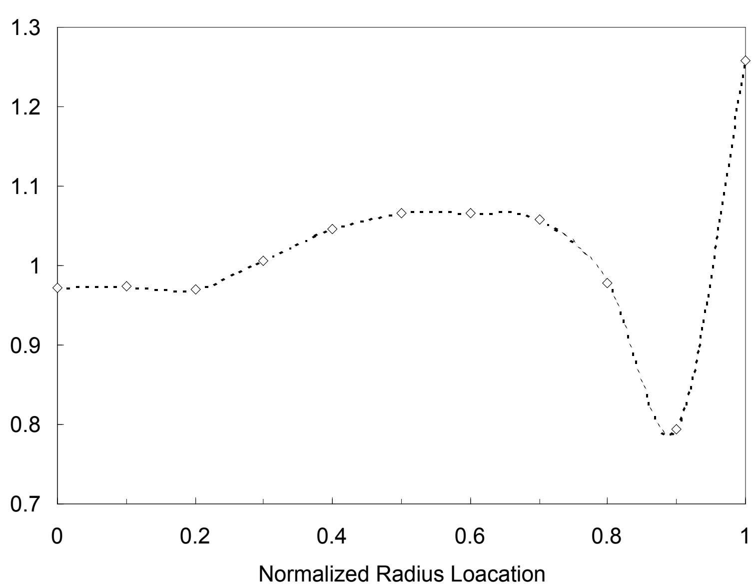

Figure 7. Normalized material removal rate across the wafer.

under a zero ring-wafer gap and different ring pressures. The simulation result when ring pressure is zero (implying without ring), correlates qualitatively well with the experimental material removal non-uniformity [**] as shown in Figure 7. In the experiment, no retaining ring is used. The platen/pad rotation speed is close to the head/wafer rotation speed, therefore, the velocity non-uniformity is minimal. The material removal non-uniformity can therefore be attributed to the pressure non-uniformity. The correlation of the simulation and experimental results implies that solid-solid contact is the dominant contact mode under the experimental conditions. From Figures 6 and 7, it is seen that while the pressure distribution on the center part of the wafer is quite uniform, a large variation is observed over the edge: decreases first and then increases rapidly at the edge of the wafer. This feature of pressure variation over the edge cannot be captured by the earlier indentation model.

To remove the edge effects, it is natural to add a retaining ring around the wafer. This ring can be considered as an extension of the wafer and the edge effects may be moved from the wafer to the ring. Based on the simulation results, for the case of zero ring-wafer gap, when the ring pressure is the same as the pressure over the wafer's top surface, the

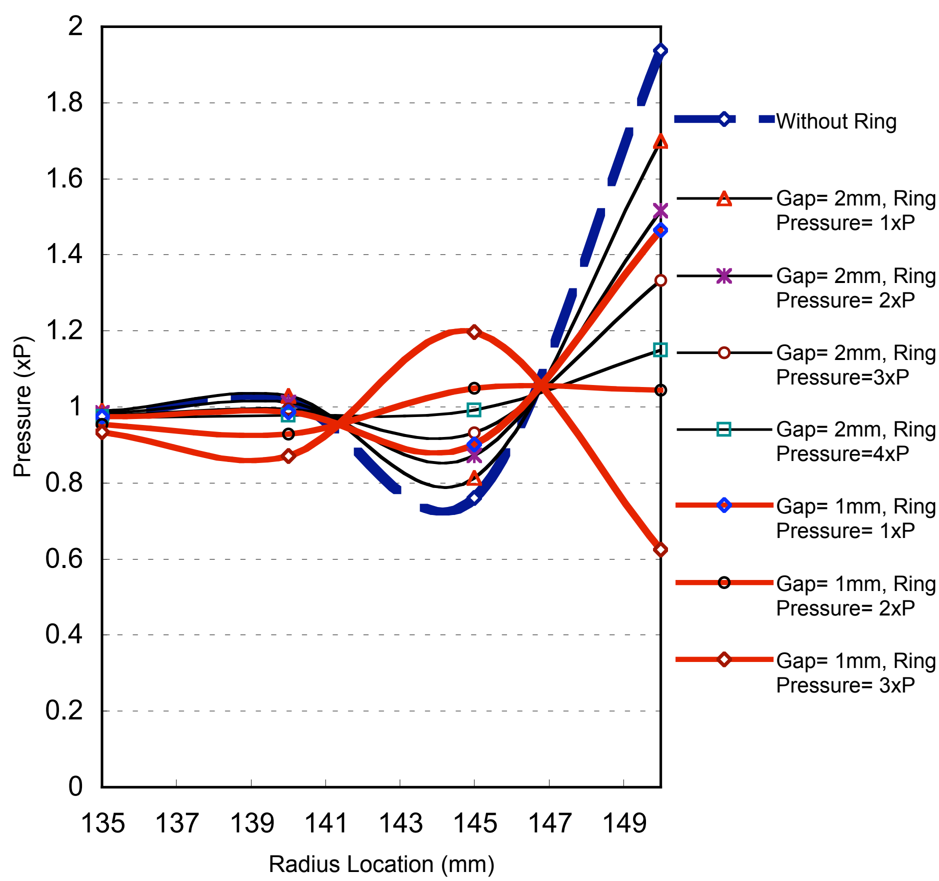

Figure 8. The effects of the retaining ring location and retaining ring pressure on the edge pressure profile.

non-uniformity is the smallest, Figure 6. A retaining ring pressure smaller than the wafer pressure *P* is not sufficient to drop the edge pressure, Figure 6. A ring pressure larger than the wafer pressure, say, 2x*P,* however, will drop the edge pressure too much, leading to a slower process at the edge, Figure 6. The simulation results here imply that an optimal ring pressure exists in terms of small edge effects.

The zero gap between the ring and wafer gap is an ideal case. Practically, the gap can never be zero considering the limitation of the manufacturing capability. Therefore, it is needed to simulate the effects of this gap on the pressure profile. Figure 8 shows the simulation results for two gaps. When the gap is 1 mm, the optimal ring pressure is $2P$. When the gap is 2 mm, the optimal ring pressure is $4P$. A larger gap needs a larger ring pressure to compensate the edge effects. This pressure should not be too large in comparison with the wafer pressure. Therefore, a gap between 0 and 1 mm may be an optimal gap considering the above tradeoffs.

In summary, the simulation results here indicate that adding a retaining ring is an effective method to reduce the edge pressure variance. The gap size and ring pressure can be adjusted simultaneously to obtain an optimal pressure profile. Similar models can be implemented using BEM to see the results of ring width, ring height and ring materials on the edge pressure improvements. They are not given here.

3.2 Solid-fluid-solid contact

In some process conditions, say, when the velocity of the wafer is large, down pressure is small or the slurry viscosity is large, a fluid film may be formed over the wafer-pad interface (see hydrodynamic region in Figure 9 of the Stribeck curve [2]). All the models

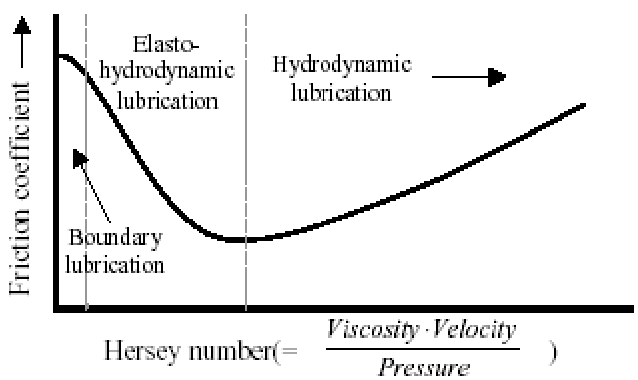

Figure 9. Stribeck curve.

in previous work [5, 6, 7] are based on the assumption of solid-solid contact. The existence of a fluid film is undesirable in terms of planarization ability. However, when low-K materials are polished, the fluid film may be preferred to avoid delamination due to the aggressive contact between wafer and pad in solid-solid contact mode. Therefore, in this section, a two dimensional (2D) model is developed to predict the pressure distribution in the case of the solid-fluid-solid contact.

Figure 10 describes the 2D wafer-slurry-pad contact model across A-B in Figure 2 considering the fluid film. The wafer surface is assumed to be flat. Both the wafer and pad are assumed to be rigid bodies and their deformation is not considered for simplification. For a more complete model that considers wafer and pad deformation, and wafer curvature, the readers are referred to [4].

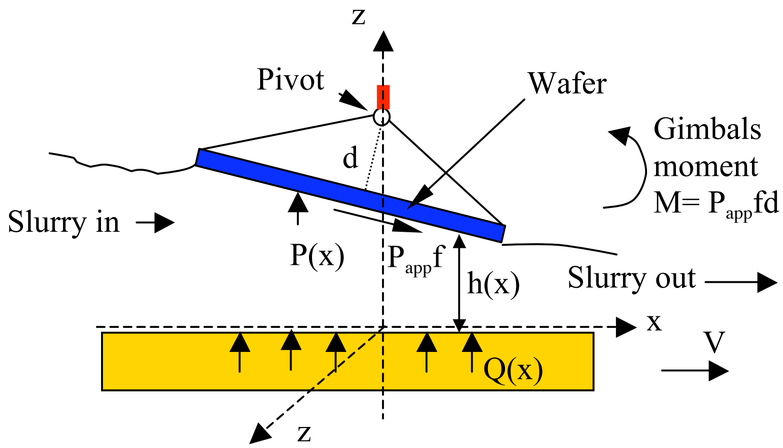

Figure 10. Two-dimensional model of wafer-slurry-pad contact in hydrodynamic lubrication mode.

The governing equation for the pressure distribution $P(x)$ in the 2D case is the Reynolds equation of lubrication theory [4]:

$$\frac{dh(x)^3 \dfrac{dP(x)}{dx}}{dx} = 6\mu U \frac{dh(x)}{dx} + Q(\mathrm{x}) \tag{7}$$

where $P(x)$ is the pressure and $h(x)$ is the thickness of the slurry film at the location x, and $Q(x)$ is the rate of the slurry flow from the bottom of the polishing pad. In a novel CMP configuration by SpeedFam (now Novellus System), the slurry is distributed from not only the side of the wafer but also from the bottom of the pad, based on the idea that non-uniform slurry distribution may be one of the contributors of the WIWNU. In this work, $Q(x)$ is assumed to be uniform across the wafer-pad interface. For a conventional machine, Q is zero. It is shown late that the magnitude of the uniform Q does not affect the pressure distribution.

Without considering the wafer and pad deformation, the slurry film thickness can be written as

$$h(x) = h_0 + \theta x \tag{8}$$

where h_0 is the slurry film thickness at the center of the wafer, and θ is the slope of the attack angle. The boundary conditions to be satisfied are

$$P(-R) = P(R) = 0 \tag{9}$$

$$\frac{1}{2R}\int_{-R}^{R} P(x)dx = P_{app} \tag{10}$$

and

$$\int_{-R}^{R} P(x)xdx = M = P_{app} fd \tag{11}$$

where Equation 9 indicates the atmospheric pressure at the inlet and outlet, Equation 10 derives from the force equilibrium condition, with P_{app} the down force applied on the wafer, and Equation 11 is from the moment equilibrium condition, where f is the friction coefficient over the wafer-slurry interface, d the distance from wafer surface to the pivot point, and $M= P_{app}fd$ the gimbals moment generated by the friction force in the x-z plane around the pivot, see Figure 10. The friction coefficient f is a function of slurry viscosity μ times velocity V, divided by pressure P (referred to as Hersey's number), as shown in Figure 9 of the Stribeck curve.

The analytical solution for the above equations 8- 11 can be obtained as:

$$P(x) = C\left(\frac{2}{1+g(\theta,h_0)x} + \frac{g^2(\theta,h_0)R^2 - 1}{(1+g(\theta,h_0)x)^2} - 1\right) \tag{12}$$

where

$$C = P_{app}g(\theta,h_0) \Big/ \left(2\ln\left(\frac{1+g(\theta,h_0)R}{1-g(\theta,h_0)R}\right) - 4Rg(\theta,h_0)\right) \tag{13}$$

$$M = fd = \int_{-R}^{R} P(x)xdx = C\left[6\frac{R}{g(\theta,h_0)} + \left(R^2 - \frac{3}{g^2(\theta,h_0)}\right)\ln\left(\frac{1+g(\theta,h_0)R}{1-g(\theta,h_0)R}\right)\right] \tag{14}$$

and $g(\theta, h_0) = \theta / h_0$ a function of the unknown values of the attack angle θ and film thickness h_0. It is difficult to obtain $P(x)$ as a function of M analytically. To obtain the relationship between $P(x)$ and M, one way is to solve equation Equation 14 to obtain $g(\theta, h_0)$ as a function of M. Then substituting $g(\theta, h_0)$ into Equation 12 to obtain the $P(x)$ as a function of M. However, the nonlinear Equation 14 cannot be solved analytically. The numerical solution has to be attempted but the convergence is a concern. An alterative way is to vary $g(\theta, h_0)$ in a reasonable range. Substituting $g(\theta, h_0)$ in Equation 12 and Equation 14, respectively, yields a corresponding moment M and a pressure distribution $P(x)$. This obtained $P(x)$ is the pressure distribution under the obtained moment M. The relationship between a series of moment M and a series of pressure distribution $P(x)$ can thus be obtained by varying $g(\theta, h_0)$. If the machine design parameter d, which is usually in the range of 20 mm - 30 mm, is known, the relationship between friction coefficient f and the pressure distribution is obtained as well. This method is much easier and used in this work. The problem with it is that film thickness parameter θ and h_0 cannot be obtained explicitly.

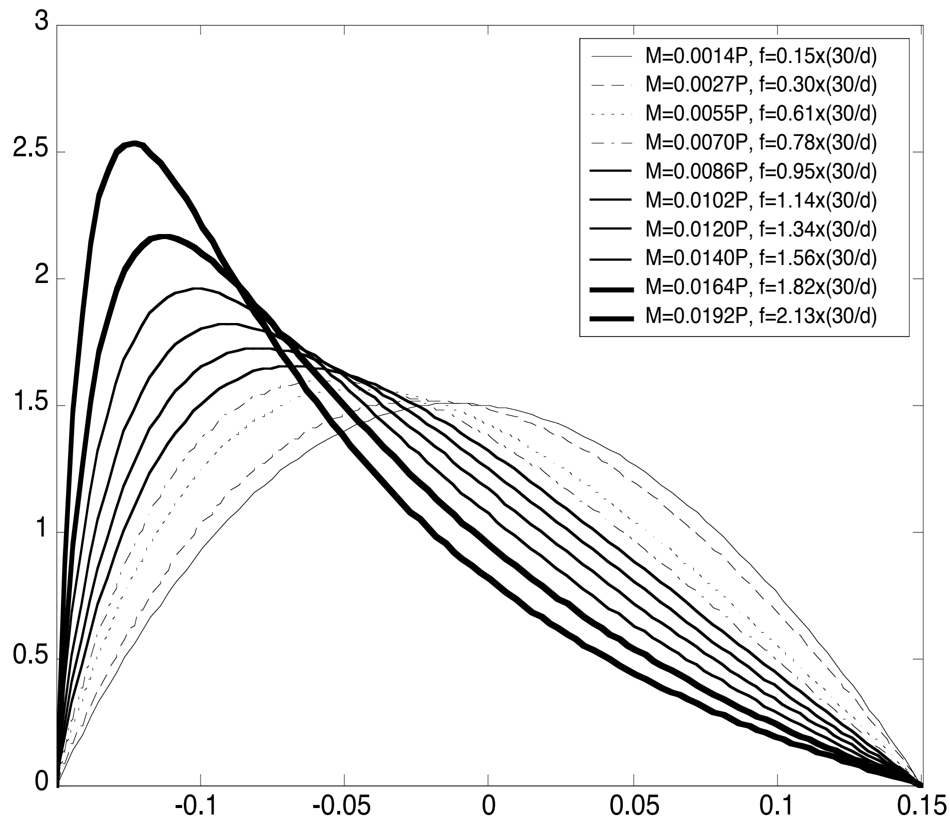

Figure 11. Asymmetric pressure distribution under different moments M or friction coefficients f for a 300mm wafer.

From the above equations, it is also seen that when Q is uniform, the pressure distribution is independent of film flow rate Q. For an arbitrary function $Q(x)$, it may affect the pressure distribution and a similar method as above can be attempted to obtain the relationship between M and $P(x)$. From Equations 12 and 14, the film viscosity μ and the relative velocity V of the wafer do not contribute directly to the pressure distribution. However, from the lubrication theory, the friction coefficient is a function of the film viscosity μ and the relative velocity V, as shown by the Stribeck curve in the hydrodynamic lubrication region of Figure 9. Therefore, their effects on the pressure distribution are reflected through the friction coefficient f or the moment M.

Figure 11 shows simulation results of the pressure distribution under different moments M or friction coefficients f for a 300 mm wafer. The number before the term $(30/d)$ is the friction coefficient for a machine with parameter d = 30mm. For a machine with an arbitrary design parameter d, the corresponding coefficients should times $30/d$. It is seen that when the friction coefficient is small, the pressure profile is symmetric. With the increase of the friction coefficient, the maximum pressure is moving from the center to the edge of the wafer and the pressure profile becomes more and more asymmetric. The asymmetric distribution of the pressure is to balance the anti-clock moment M in the *x-z* plane.

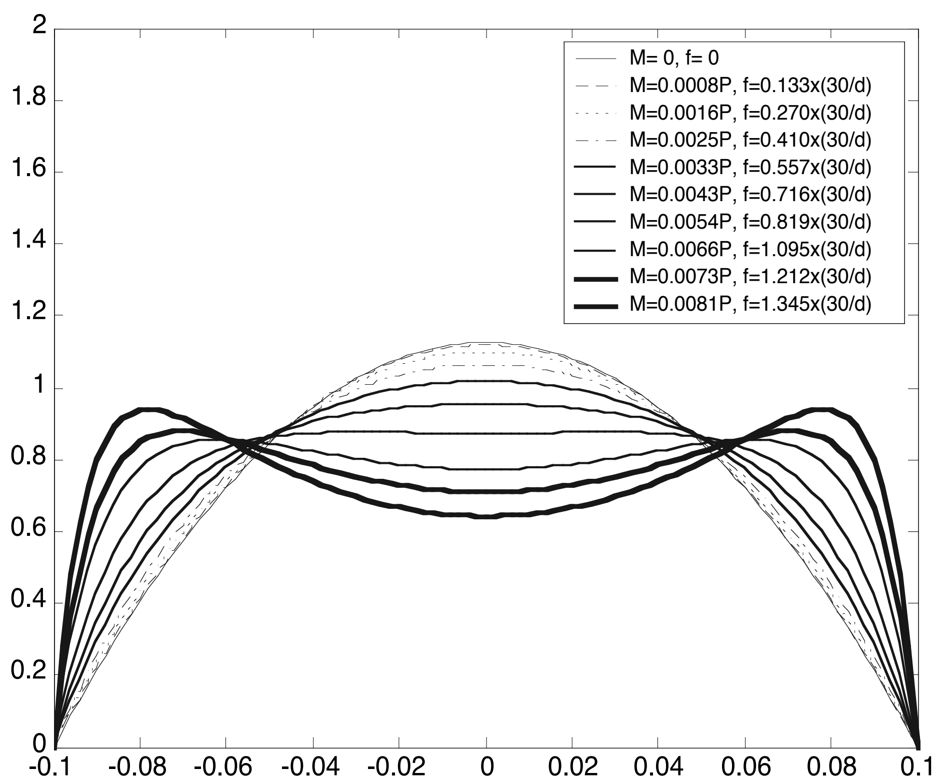

Figure 12. Average pressure distribution under different moments M or friction coefficients f for a 300mm (12 inch) wafer.

The rotation of the wafer around its center in *x-z* plane will average out the asymmetric distribution of the pressure. Figure 12 shows the simulation results of the average pressure for a 300 mm wafer. It is seen that when the moment M or the friction coefficient f is small, the pressure distribution is like a bow, center high and edge low.

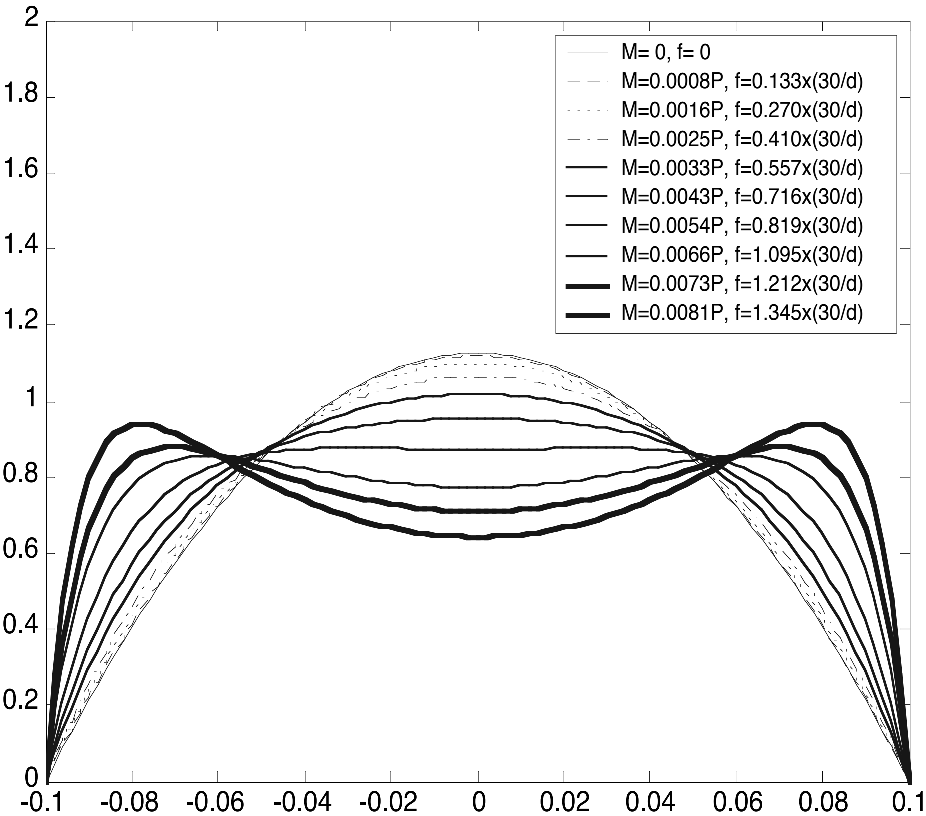

Figure 13. Average pressure distribution under different moments M or friction coefficients f for a 200mm (8 inch) wafer.

With the increase of the moment, the pressure distribution profile becomes smoother in the center, with the maximum pressure moving to the edge of the wafer. When the moment is larger than a certain value, a reverse bow will be formed at the center. In terms of smaller non-uniformities, M in the range of $0.0102P$ ~ $0.0164P$ is preferred from Figure 12. This corresponds to friction coefficients *f* in the range of 1.14~1.82 for a d of 30mm and 1.14~1.82x(30/d) for an arbitrary d. Similar simulations are done for 200mm (8 inch) and 150mm (6 inch) wafers. The pressure profiles are shown in Figures 13 and 14, respectively. Suggested ranges of friction coefficients are given as 0.82~1.21x(30/d) and 0.57~0.91x(30/d). For a smaller wafer size, the optimal friction coefficients are smaller. The above results yield the favorite range of friction coefficients for a machine design parameter d in the range of 10~85 mm, as shown in Figure 15. Combining Figures 15 and 9 (Stribeck curve of friction coefficients), the process window of down pressure P and relative velocity V can be obtained.

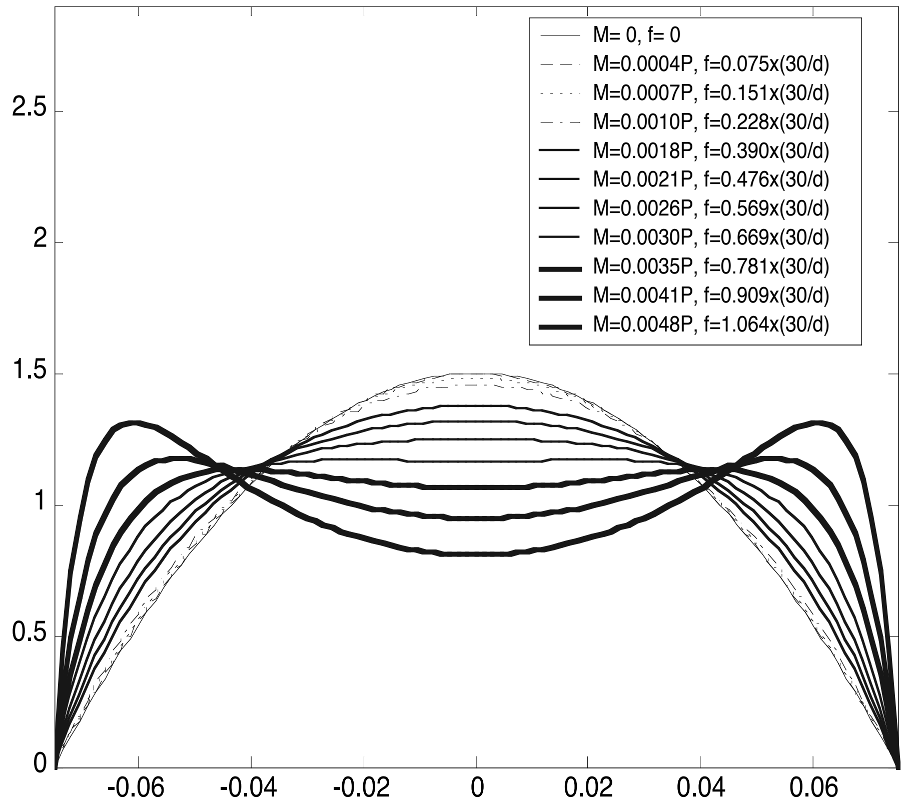

Figure 14. Average pressure distribution under different moments M or friction coefficients f for a 150mm (6 inch) wafer.

There are two usages of Figure 15. One is mentioned above. When the machine design parameter d is known, the process parameters, including the pressure P, velocity V, and consumable parameters such as slurry viscosity, μ can be adjusted so that the friction coefficients f fall in the desired region. When the process is fixed, say, P, V, and μ have been optimized based on other requirements, such as the minimum dishing and erosion in the copper damascene process, and therefore, the friction coefficient f is fixed, Figure 15 can be used to find the optimal machine design parameter d. This gives feedback to the machine designer and may lead to a modification of the machine configurations. In some cases, multi polishing heads with different d may be supplied by the equipment vendor to the IC manufacturers. Figure 15 can help them find the correct polishing head for a fixed process.

A final question is whether the retaining ring will alleviate the edge effects. From the above analysis, it is possible, since the retaining ring moves the zero atmosphere pressure to the edge of the ring. Simulations can be done using Equations 12, 13, and 14, by replacing R with R plus ring size.

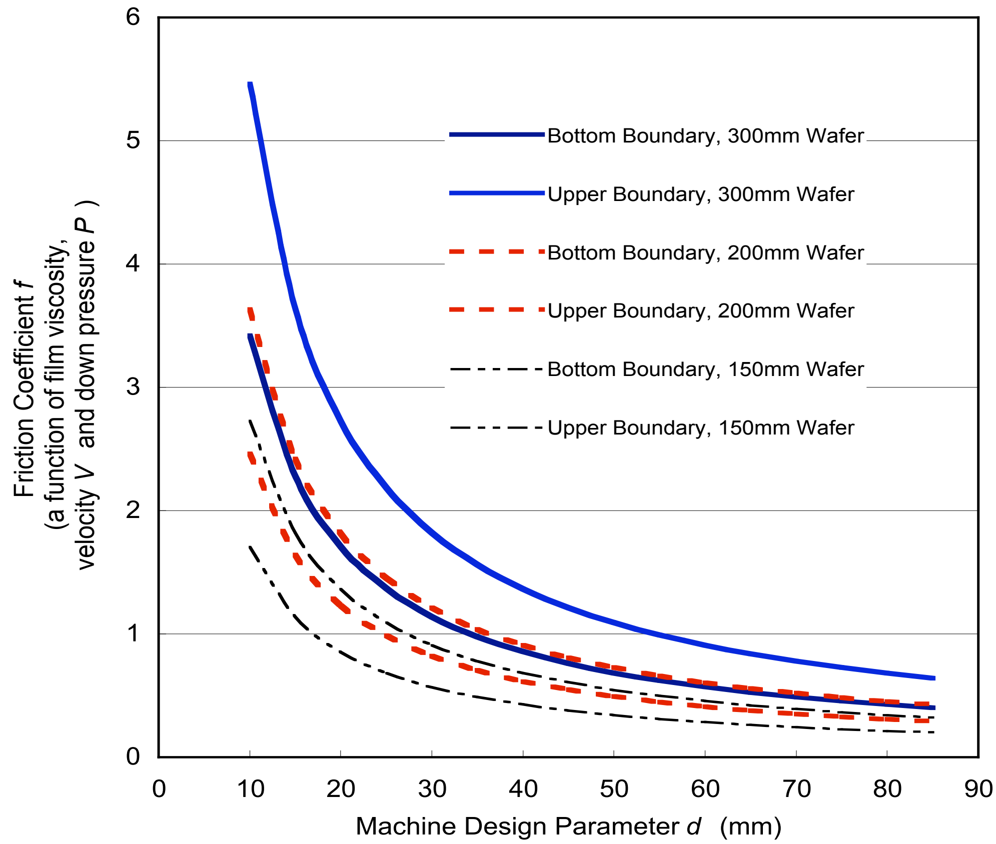

Figure 15. Suggested range of friction coefficients f for different machine design parameter d.

4. Optimization of WIWNU from the viewpoint of consumable effects

In the earlier sections, the optimization of WIWNU is discussed from the viewpoint of pressure distribution and velocity distribution. An alternative method [8], based on Equation 2, is to reduce the sensitivity of material removal rate on the pressure distribution by changing Preston's coefficient K_e and MRR_o. This idea can be shown schematically in Figure 16. Lines 1, 2, and 3 represent a revised Preston's equation $MRR = K_{pe}PV + MRR_0$ under three different consumable recipes. Suppose that the velocity is uniform, the average down pressure over the wafer surface is P_{avg}, the maximum pressure is P_{max},, and the minimum pressure in P_{min}, and this pressure distribution does not change with the consumable recipes. Then, apparently, using Equation 2, the non-uniformity is smaller under recipes 1 and 3 than that under recipe 2.

Changing K_e and MRR_0 in Equation 2 actually requires the change of C_1 and C_2 in the material removal rate, Equation 21 developed in [5]. Substitution of it into non-uniformity Equation 2 yields

$$
\text{WIWNU} = \frac{MRR_{max} - MRR_{min}}{MRR_{avg}}
$$

$$
= \frac{C_1(1-\ddot{O}\left(3-C_2 P_{max}^{\frac{1}{3}}\right)\sqrt{P_{max}} - C_1(1-\ddot{O}\left(3-C_2 P_{min}^{\frac{1}{3}}\right)\sqrt{P_{min}}}{C_1(1-\ddot{O}\left(3-C_2 P^{\frac{1}{3}}\right)\sqrt{P}\,V}
$$

$$
= \frac{(1-\ddot{O}\left(3-C_2 P_{max}^{\frac{1}{3}}\right)\sqrt{P_{max}} - (1-\ddot{O}\left(3-C_2 P_{min}^{\frac{1}{3}}\right)\sqrt{P_{min}}}{(1-\ddot{O}\left(3-C_2 P^{\frac{1}{3}}\right)\sqrt{P}} \tag{15}
$$

It is seen from Equation 15 that only parameters related to C_2 influence the WIWNU. These include: *Pad Material, Pad Topography* and *Abrasive Size Distribution*. Ideally, the production rate should not be sacrificed for an improvement of WIWNU. Therefore, the average material removal rate should be increased or kept unchanged after the WIWNU improvement. (This means a change of consumable recipe from 3 to 1 in Figure 16 is undesirable, even with a WIWNU improvement.) An increase of C_1 can lead to a larger average material removal rate. However, it is worthy to note that a mathematical analysis of Equations 15 and 21 in [5], reveals that the minimum WIWNU that can be realized by changing C_2 (or optimizing consumable parameters) is $0.5(P_{\max}-P_{\min})/P_{avg} \times 100\%$ if MRR_{avg} remains unchanged. When increasing MRR_{avg}, the minimum WIWNU that can be realized is even larger.

Based on the above discussions, a three-step process can be used to improve WIWNU:

1. Optimize the consumable parameters, including pad topography, pad material, and abrasive size, to decrease the value of C_2 until the WIWNU requirement is satisfied.

2. Check the average material removal rate. If it is not smaller than that before the adjustment, the optimization is successful.

3. If the average removal rate after the adjustment becomes smaller, increase the density of slurry, dilution ratio, slurry abrasive weight concentration, slurry oxidizer concentration, relative velocity, and other parameters, which should not negatively influence the already improved WIWNU, to increase the *MRR*.

Increasing the density of slurry, dilution ratio of slurry, slurry abrasive concentration, and slurry chemical concentration in step 3 above, however, implies a more expensive process. This may be undesirable from the viewpoint of cost of ownership (CoO). The pad topography, pad material and abrasive size distribution influence the WIWNU (C_2) and *MRR* simultaneously. Therefore, by selecting proper pad topography and abrasive size distribution parameters, an optimization may be realized without step 3 and this leads to lower costs. The effects of pad topography, pad materials and abrasive size distribution in both *MRR* and WIWNU imply that it is critical to keep them constant to realize a reproducible and controllable CMP process.

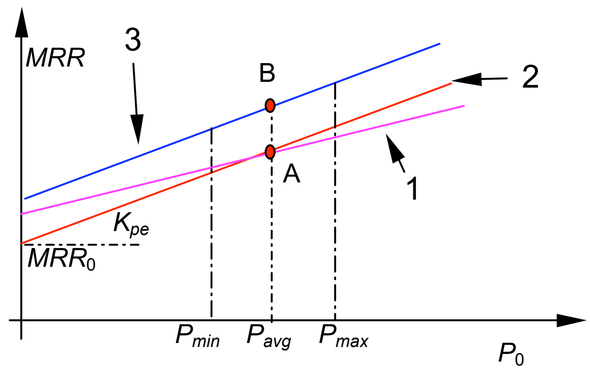

Figure 16. The material removal rate equation for different consumable.

5. Conclusion

In this report, the with-in wafer non-uniformity and its optimization are discussed from both the machine side and consumable side. At the machine side, the pressure distribution and velocity distribution are the major reasons of the non-uniform material removal rate across the wafer. The velocity distribution for the rotational type and linear type of machines are analyzed systematically. The rotational part of the velocity is the contributor of the velocity non-uniformity. The pressure non-uniformity in both cases of the solid-solid contact and the solid-fluid-solid contact are discussed. Adding the retaining ring is an effective way to reduce the pressure non-uniformity at the edge of the wafer in the solid-solid contact mode. In the solid-fluid-solid contact mode, the friction coefficient is identified as the major contributor to the non-uniformity. A process window of pressure and velocity in terms of small non-uniformity can be obtained by combining the model proposed in this report and the Stribeck curve of the friction coefficients. At the consumable side, a systematic method can be applied to optimize the WIWNU in solid-solid contact mode based on the material removal model developed in previous investigations [5, 6, 7].

References

[1] K. L. Johnson, *Contact Mechanics*. Cambridge, Cambridge University Press, 1985.

[2] Y. Moon, "Mechanical aspects of the material removal mechanism in chemical mechanical polishing (CMP)," Ph.D. Thesis, Department of Mechanical Engineering, University of California at Berkeley, Berkeley, CA, U. S. A., 1999.

[3] J. F. Luo, Y. J. Liu and E. J. Berger, "Analysis of two-dimensional thin structures (from micro- to nano-scales) using the boundary element method," *Computational Mechanics*, Vol. 22, No. 5, pp. 404-412, 1998.

[4] D. G. Thakurta, C. L. Borst, D. W. Schwendeman, R. J. Gutmann, W. N. Gill, "Pad porosity, compressibility and slurry delivery effects in chemical-mechanical planarization: modeling and experiments," *Thin Solid Films*, Vol. 366, No. 1-2, pp.181-190, 2000.

[5] J. Luo and D. A. Dornfeld, "Material removal mechanism in chemical mechanical polishing: theory and modeling," *IEEE Transactions on Semiconductor Manufacturing*, Vol. 14, No. 2, pp. 112-123, 2001.

[6] J. Luo and D. A. Dornfeld, "Material removal regions in chemical mechanical planarization for sub-micron integrated circuit fabrication: coupling effects of slurry chemicals, abrasive size distribution and wafer-pad contact area," *IEEE Transactions on Semiconductor Manufacturing*, Vol. 16, No. 1, pp. 45-56, 2003.

[7] J. Luo and D. A. Dornfeld, "Effects of abrasive size distribution in chemical mechanical planarization: modeling and verification," *IEEE Transactions on Semiconductor Manufacturing,* in press, 2003.

[8] J. Luo and D. A. Dornfeld, "Optimization of chemical mechanical planarization from the viewpoint of consumable effects," *Journal of the Electrochemical Society*, in press, 2003.